AGU PUBLICATIONS

JGR

Journal of Geophysical Research: Solid Earth

RESEARCH ARTICLE
10.1002/2016JB013027

Special Section:
Slow Slip Phenomena and Plate Boundary Processes

Comparative study of tectonic tremor locations: Characterization of slow earthquakes in Guerrero, Mexico

J. Maury[1], S. Ide[1], V. M. Cruz-Atienza[2], V. Kostoglodov[2], G. González-Molina[2], and X. Pérez-Campos[2]

[1]Earth and Planetary Science, University of Tokyo, Tokyo, Japan, [2]Instituto de Geofísica, Universidad Nacional Autónoma de México, Mexico City, Mexico

Key Points:
- Two seismic networks provide tremor catalogs with different resolutions
- Moment tensors of slow earthquakes in Guerrero are consistent with plate motion
- Matched filtering detected 11 VLF events accompanying tremors

Supporting Information:
- Supporting Information S1

Correspondence to:
J. Maury,
maury@eps.s.u-tokyo.ac.jp

Citation:
Maury, J., S. Ide, V. M. Cruz-Atienza, V. Kostoglodov, G. González-Molina, and X. Pérez-Campos (2016), Comparative study of tectonic tremor locations: Characterization of slow earthquakes in Guerrero, Mexico, *J. Geophys. Res. Solid Earth*, *121*, doi:10.1002/2016JB013027.

Received 24 MAR 2016
Accepted 7 JUL 2016
Accepted article online 9 JUL 2016

Abstract Deep tectonic tremor in Guerrero, Mexico, has been observed using dense temporal seismic networks (i.e., the Meso-American Subduction Experiment and Guerrero Gap Experiment (G-GAP) arrays) during two different time periods. We apply a set of seismic waveform analysis methods to these data sets to constrain the locations of tremors and determine the associated moment tensors. First we detect and locate the tremors. Next, very low frequency (VLF) signals are identified by stacking waveform data during tremor bursts, and their moment tensors are determined. Finally, to better investigate the link between tremors and VLF earthquakes, we detect VLF events using a matched filtering algorithm to search continuous seismic records. None of the 11 VLF events detected by this method occurred in the absence of tremor bursts suggesting they are indeed part of the same phenomena. Unlike previous investigations, our results for the G-GAP period reveal that downdip tremor activity (i.e., in the so-called "sweet spot") is segmented into two patches separated by 40 km in the along-trench direction, indicating possible variations in the geometry of the plate interface and/or slab effective pressure. Moment tensors of VLF signals are consistent with shear slip on the near-horizontal plate interface, but source depths are about 5 km deeper than the established plate interface. The slip directions of the VLF events are slightly (~10°) counterclockwise of the plate convergence direction, indicating that strain energy promoting left-lateral strike-slip motion may accumulate in the continental crust during the interseismic period.

1. Introduction

Deep tectonic tremors that accompany slow slip events (SSEs) were discovered almost simultaneously in two regions: Cascadia [*Rogers and Dragert*, 2003] and Japan [*Obara*, 2002]. Later, *Shelly et al.* [2007], when studying low-frequency earthquakes (LFEs), proposed that nonvolcanic tremors, or tectonic tremors observed between 1 and 15 Hz, could be merely a superposition of LFEs. Very low frequency (VLF) earthquakes detected in the 0.02–0.05 Hz frequency band present intermediary duration scale between tremors, LFEs, and SSEs, with durations between days and years [*Ito et al.*, 2007]. Many more recent studies have investigated the characteristics of these signals [*Schwartz and Rokosky*, 2007; *Peng and Gomberg*, 2010; *Beroza and Ide*, 2011]. Slow earthquakes consist of long-duration deformation signals with low-amplitude seismic waves. One of their distinguishing characteristics is that their seismic moments scale with their durations, contrary to fast earthquakes seismic moments that scale with their cubic durations [*Ide et al.*, 2007a]. Much remains to be understood about slow earthquakes and the relationships among the different types of events. For example, why, with comparable networks, are only SSEs and VLF earthquakes found in some places (e.g., Boso), while in other regions (e.g., Nankai), all known types of slow earthquakes are present [*Beroza and Ide*, 2011]? Do slow earthquakes occur in every subduction zone? To answer these questions, and better characterize slow earthquakes, studies of different subduction zones are needed.

Locating tremors is not easy because there are no clear *P* or *S* arrivals. Various methods have been implemented to circumvent this problem: the better known examples include envelope correlation [*Obara*, 2002; *Ide*, 2010], source scanning algorithms [*Kao et al.*, 2005], the use of differential *P* and *S* arrival times [*La Rocca et al.*, 2009], LFE detection [*Shelly et al.*, 2007; *Brown et al.*, 2008], and tremor energy and polarization methods [*Cruz-Atienza et al.*, 2015]. Most of these methods have been successfully applied in Cascadia and Japan because of the availability of well-distributed seismological networks. Along with other techniques, they have been subsequently applied to other subduction zones in locations such as Mexico [*Payero et al.*, 2008; *Husker et al.*, 2012], Costa Rica [*Brown et al.*, 2009], and Taiwan [*Peng and Chao*, 2008], as well as transform faults in

California [*Nadeau and Dolenc*, 2005]. In some places (Nankai, Cascadia), tremors occur in the same areas as SSEs [*Obara et al*., 2004; *Brudzinski and Allen*, 2007], while in others (Mexico, Costa Rica, and New Zealand) they are located slightly apart from each other [*Kostoglodov et al*., 2010; *Outerbridge et al*., 2010; *Ide*, 2012]. Thus, we wonder how sparser station networks impact tremor detection and location. Assessing the robustness of these locations, and the corresponding location techniques, is a key goal of this study.

Once the locations of slow earthquakes are known, we need to consider what their mechanisms are and whether they are the same for all classes of slow earthquakes. It has been suggested that deep tectonic tremors occur as a result of shear slip on the plate interface [*Wech and Creager*, 2007; *Ghosh et al*., 2009; *Cruz-Atienza et al*., 2015]. However, since tremor signals are extremely emergent, it is difficult to constrain their moment tensors and their vertical location very precisely. *Shelly et al*. [2007] demonstrated that tremors are composed of LFE swarms, meaning that complete focal mechanism solutions can be obtained for individual LFEs [*Ide et al*., 2007b]. These LFEs have been clearly located on the plate interface [*Shelly et al*., 2006; *Brown et al*., 2009]. Focal mechanisms have then been determined for LFEs in Cascadia [*Royer and Bostock*, 2014], Nankai [*Imanishi et al*., 2016], and Mexico [*Frank et al*., 2013]. Focal mechanisms for VLF events have also been determined for isolated events in the Nankai [*Ito et al*., 2007, 2009] and Ryukyu subduction zones [*Ando et al*., 2012]. More recently, *Ide and Yabe* [2014] used a stacking method to detect VLF events occurring simultaneously with tremors and determined their corresponding focal mechanisms, with results that corroborate the hypothesis that slow earthquakes all arise from the same physical phenomena. However, focal mechanisms must be resolved for tremor samples from other locations before such general conclusions can be accepted.

This study focuses on the Guerrero region of Mexico, where the Cocos plate is subducting beneath the North American plate at the Middle America Trench. Many subduction thrust earthquakes have occurred along the Mexican coast with a recurrence time of 30–60 years except in the so-called "Guerrero Gap," where the most recent $M_w \sim 7.5$ earthquake in the region occurred in 1911. Every 4 years, long-term SSEs occur downdip of the Guerrero Gap seismogenic interface (Figure 1a), with a total moment magnitude of 7.5, making these the largest SSEs detected to date in subduction zones [e.g., *Kostoglodov et al*., 2003; *Iglesias et al*., 2004; *Larson et al*., 2007; *Radiguet et al*., 2012]. These are thought to enable the aseismic release of most of the strain energy that accumulates in the seismogenic zone [*Radiguet et al*., 2012]. Tectonic tremors have also been detected downdip of the SSEs [*Payero et al*., 2008], occurring over a wide area and separated into two patches in the subduction direction [*Husker et al*., 2012; *Cruz-Atienza et al*., 2015], a feature that is uncommon in other subduction zones. The updip tremor patch is active mainly during the long-term SSEs, while the downdip patch, often called the "sweet spot" [*Husker et al*., 2012], is active almost continuously. Detections of LFEs support these findings and suggest that short-term SSEs downdip of long-term ones could be related to this second tremor patch [*Frank et al*., 2014, 2015]. Another unique characteristic of Guerrero is that the subduction interface is subhorizontal for nearly 200 km (Figure 1). Slow earthquakes occur predominantly in this flat part of the subducting slab.

This study has two main aims. First, we compare tremor locations obtained from two temporal networks with very different spatial configurations. Second, we determine the moment tensors of tremors using stacked waves in the VLF band, as has been done in Japan [*Ide and Yabe*, 2014] and Taiwan [*Ide et al*., 2015]. This provides a vastly more complete picture of the tremor source mechanism in Guerrero, since previous studies have resolved only rake directions [*Cruz-Atienza et al*., 2015], with one complete focal mechanism estimated for the entire area [*Frank et al*., 2013]. In addition, we search for individual VLF events using a matched filtering algorithm, to determine the temporal correlation (if any) between VLF events and tremors.

2. Seismic Data

We analyze slow earthquakes in Guerrero in two time periods between 2005 and 2012, corresponding to two different temporary network deployments. During these time periods, two analyses are performed: tremors are located and moment tensors of stacked VLF signals are determined. For high-frequency tremor detection, every available station is used. Moment tensor calculations in the VLF band (0.02–0.05 Hz) use only data from broadband sensors.

During the first time period, from January 2005 to June 2007, the data analyzed are from broadband sensors deployed during the Meso-American Subduction Experiment (MASE) [*Meso-American Subduction Experiment*,

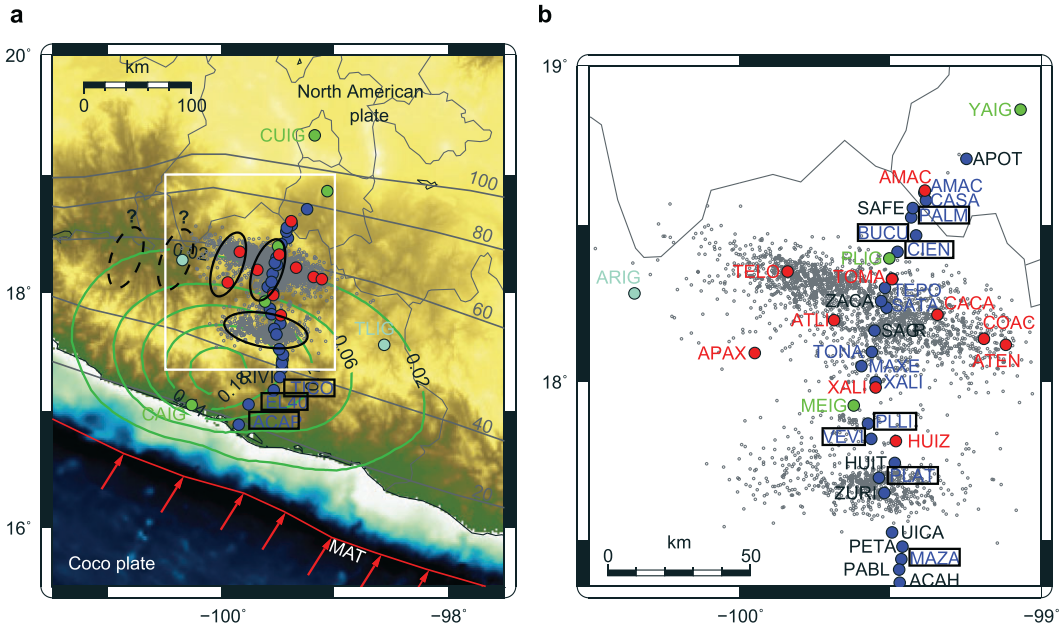

Figure 1. Study area in Guerrero, Mexico, showing station distributions for each experiment. (a) Seismotectonic map. Grey circles indicate tremors located with the MASE array. The slip distribution of the 2006 SSE is shown in green isocontours with 0.04 m spacing [*Radiguet et al.*, 2011]. Tremor clusters found in this study are indicated by black ellipses. Other potential clusters are indicated by dashed black ellipses. Red arrows show the direction of convergence. Isodepth contours of the subduction zone interface are indicated by grey lines [*Pardo and Suarez*, 1995]. (b) Enlargement of the area outlined by the white rectangle in Figure 1a. MASE stations are plotted as blue circles; G-GAP stations are shown as red circles. Green circles are permanent SSN stations installed before the MASE experiment; permanent stations installed after the MASE experiment are indicated by cyan circles. MASE station names in blue are used for VLF stacking. MASE station names framed by black rectangles are used to search for isolated VLF events.

2007]. For the tremor locations, 29 of 100 network stations are selected, based on their proximity to the region of interest. For moment tensor determination, 17 sensors are selected, based on their relatively high signal-to-noise ratios in the VLF band. Since the original purpose of the MASE project was a structural survey, all seismometers were deployed in a linear configuration almost perpendicular to the trench (Figure 1).

During the second time period, from November 2009 to mid-2012, seismograms from 35 vertical-component short-period sensors and three medium-period three-component sensors from the G-GAP experiment are used for tremor location. These instruments are localized around the "sweet spot"; each red circle in Figure 1 corresponds to a miniarray with six sensors separated by less than 1 km.

In addition, broadband seismic data from the permanent network of the Servicio Seismológico Nacional (SSN) are used for both analyses. Two permanent stations, ARIG and TLIG, were added between the two temporary deployments, located on either side of the "sweet spot" (Figure 1), thereby improving the network coverage for the second study. Tremor detectability and focal mechanism reliability changed with time due to this varying stations availability (Figure 2e). During the first time period, the network is linear but consists of broadband stations; during the second time period, the network provides good azimuthal coverage around the sweet spot but has few broadband stations. Assuming that the tremor signals are mainly *SH* waves, horizontal components should be used. However, the G-GAP temporary network is composed primarily of vertical-component sensors; thus, for the second time period, vertical components are used for sensors with no horizontal component (35 of 38 stations).

3. Methods

To detect and locate tremors, we use 34 stations from the first time period and 45 stations from the second. We apply an envelope correlation method [*Obara*, 2002; *Ide*, 2010] to detect the events. The signals are band passed between 2 and 8 Hz, squared, low-pass filtered at 0.2 Hz, and resampled at one sample per second.

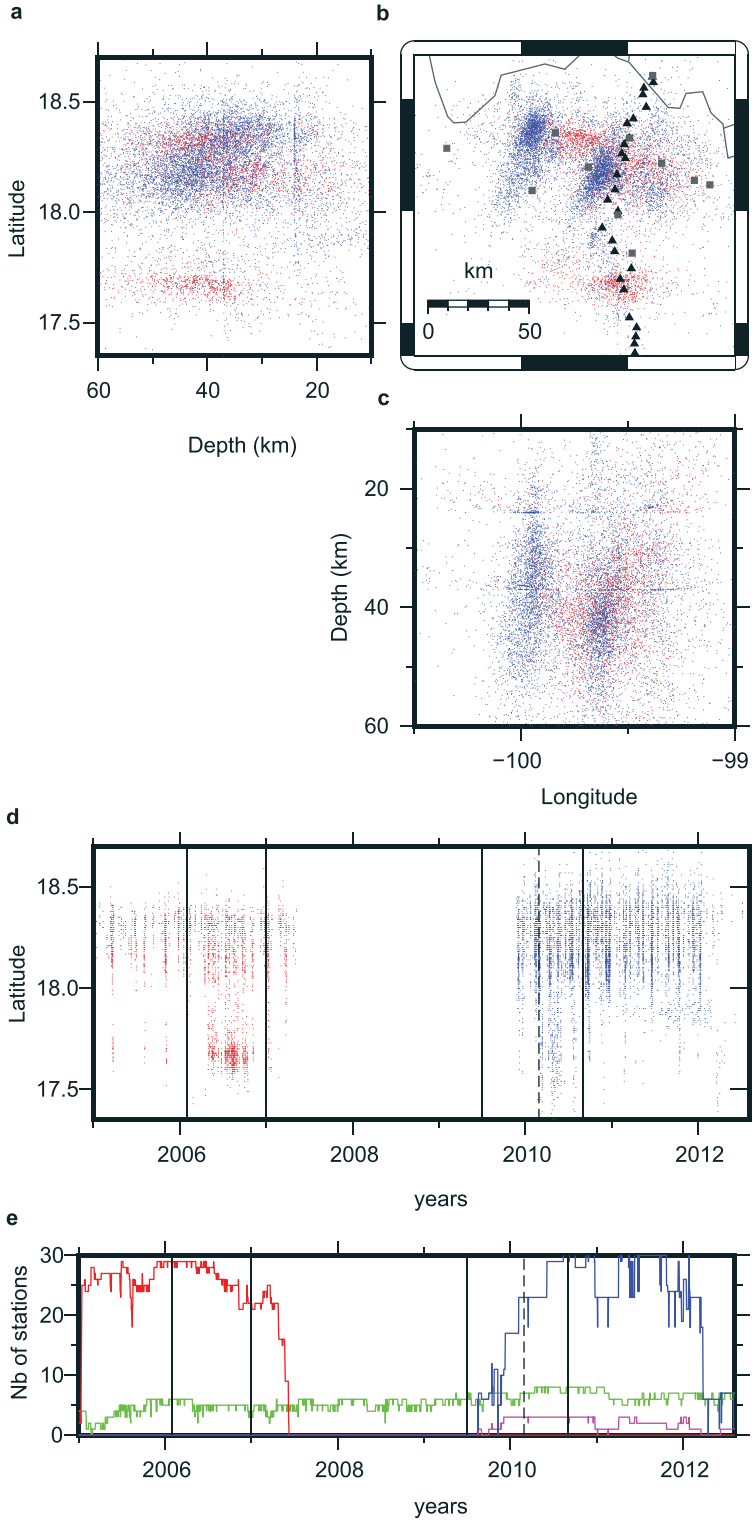

Figure 2. Tremor distribution. Tremors detected during the MASE time period are plotted in blue, while those detected during the G-GAP time period are plotted in red. (a) Tremor centroids projected onto a north-south cross section. (b) Plane view of the tremor distribution. (c) East-west cross section. (d) Space-time plot of tremors. The black lines indicate the beginning and end of the 2006 and 2009–2010 SSEs. The dashed line shows the time of occurrence of the 27 February 2010 M_w8.8 Maule earthquake. (e) Station availability as a function of time. The MASE stations are indicated in red, the G-GAP vertical short-period and three-component stations are indicated in blue and magenta, respectively, and the permanent stations are indicated in green.

The envelope is approximated as the square root of the resampled data, following *Ide* [2010]. We use 5 min time windows with 2.5 min of overlap between successive calculations. A detection is declared when at least eight normalized cross correlations reach the threshold value of 0.6. For the G-GAP time period, correlations between stations within the same miniarrays are not considered. To locate the detected tremors, we solve a nonlinear inverse problem that minimizes the squared misfit between observed and calculated travel times [*Ide*, 2010]. A velocity model obtained from *S* wave tomography by *Iglesias et al*. [2010] is used for location, completed by the AK135 1-D velocity model [*Kennett et al*., 1995] for the deeper part. A clustering technique is applied to reject outliers and false detections: only events that are within a space-time window of 10 km and 1 day with at least one other event are kept. Moreover, events at latitudes less than 17.35° are rejected, because most of these events are earthquakes.

In addition, to confirm our tremor locations, we also apply the Tremor Energy and Polarization (TREP) method [*Cruz-Atienza et al*., 2015] to locate tremor sources using the G-GAP array. Given tremor detections by means of a spectral threshold strategy [*Husker et al*., 2010], the TREP method simultaneously determines the locations and rake angles of double-couple tremor sources that explain both the spatial distribution of energy (in all three components) and the azimuth of the particle motion polarization ellipsoid. A grid search is performed in a 3-D regular lattice below the array. For each node of the lattice, a time scan is performed using 1 min moving windows with 20 s overlap.

Since moment tensors of tremors are difficult to estimate, we next attempt to identify VLF signals and invert these for their moment tensors. A grid of reference points, separated by 11 km in the strike-parallel and strike-perpendicular directions, is prepared for the tremor centroid region. Seismograms are stacked at the time of occurrence for all tremors within 10 km of a reference point. If the number of tremors exceeds 100 (200 for the G-GAP time period), they are stacked in the VLF band; note that a larger number of tremors is needed for G-GAP time period because fewer stations are available. The relative amplitude of the stacked signal at the *j*th station is given by

$$u_j^s(t) = \frac{\sum_i u_{ij}(t)/A_i}{\sum_1 1/A_1}, \tag{1}$$

where $u_{ij}(t)$ is the velocity from the *i*th tremor at the *j*th station and A_i represents the relative amplitude of the *i*th event determined during an outlier control procedure. For further details, see *Ide and Yabe* [2014]. Once these signals are stacked, we estimate their deviatoric moment tensor with five basis vectors M_i, by assuming that the stacked velocity can be expressed as

$$u_j^s(t) = \sum g_{ij}(t)M_i + e_j(t)/W_j, \tag{2}$$

where g_{ij} is the theoretical waveform for a unit source of the *i*th moment tensor component, e_j is the Gaussian-distributed error, and W_j is a weighting factor. The velocity structure used for tremor detection is also used for estimating g_{ij}. The weighting factor corresponds to the inverse of the maximum amplitude of the noise in a 400 s time window before the event. Components with a noise level higher than 10 times the lowest noise level are not used. The best solution is obtained by maximizing the variance reduction,

$$VR = 1 - S(M)/S(0) = \left\| W_j u_j^s(t) - \sum_i W_j g_{ji}(t) M_i \right\|^2 \tag{3}$$

as a function of depth and source duration.

We do not try to retrieve the isotropic component of the moment tensor, because we do not have sufficient resolution. However, we consider this component small, as is the case for well-constrained VLF moment tensors in Japan [*Ide and Yabe*, 2014]. During the MASE time period, the network is linear and therefore cannot adequately constrain some parts of the moment tensor. During the G-GAP time period, only seven stations are available, with five of these aligned, also limiting the resolution.

4. Tremor Location

A total of 2990 tremors are detected during the first time period (MASE, 29 months) and 5317 tremors during the second (G-GAP, 32 months). The higher number of detections during the G-GAP time period is due to the longer time period and more optimal array geometry.

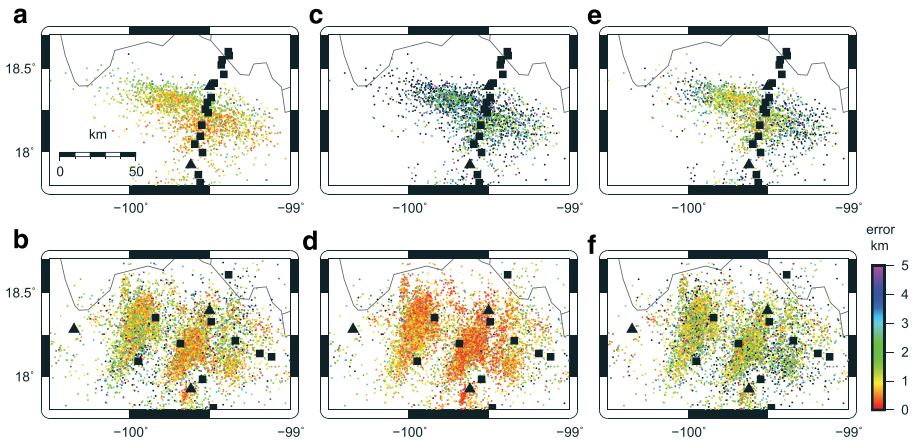

Figure 3. Standard deviations of tremor locations in the "sweet spots" region (Figure 2b). The colors indicate location errors in kilometers. (a and b) Errors in latitude, (c and d) errors in longitude, and (e and f) errors in depth. Figures 3a, 3c, and 3e are locations of MASE data; Figures 3b, 3d, and 3f are locations of G-GAP data.

Figure 2 shows the tremor locations obtained for both time periods. Even if the extent of the locations is similar, the distributions of tremor locations differ considerably between the two data sets. Using the MASE data, the two clusters already identified by *Husker et al.* [2012] and defined by *Frank et al.* [2014] are clearly visible: updip in the transient zone and downdip in the sweet spot. The G-GAP time period gives more details on the sweet spot, which appears to constitute two distinct locations in the along-strike direction, separated by ~40 km (the distance between the locations of the maximum number of tremors in each cluster). These two clusters are elongate in the dip direction and extend beyond the distributions determined using MASE time period data. The depth of the tremors is the least well-constrained parameter, as is apparent from the wide range of results obtained (Figures 2a and 2c). However, the mean depth is 38 with a standard deviation of ±11 km for both data sets, which falls within the range reported in previous studies [*Frank et al.*, 2014; *Cruz-Atienza et al.*, 2015]. An apparent east-west depth trend is observable in the MASE locations, with tremors located deeper in the western part of the cluster (Figure 2c, blue circles). This trend is probably an artifact linked to the network configuration.

The standard deviations of the model covariance matrix, calculated for the estimated parameters (Figure 3), characterize the location errors. While the errors in latitude are comparable for both time periods, the errors in longitude are greater for the MASE time period (mean of 4 km) than for the G-GAP time period (0.8 km). In

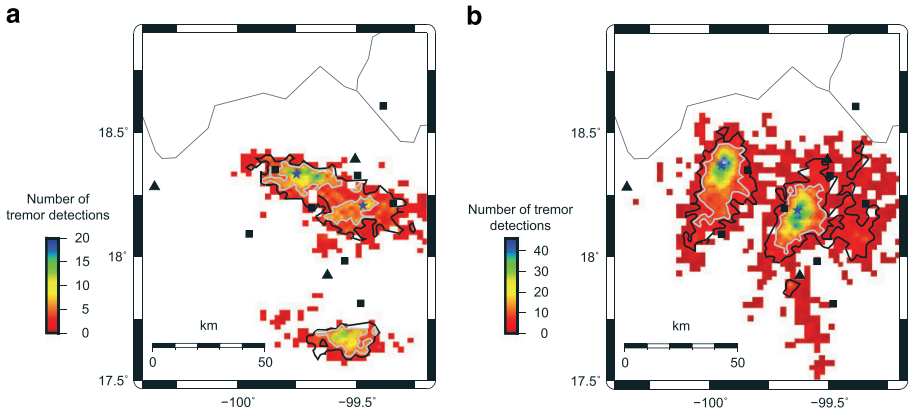

Figure 4. Maps of tremor density. The area is divided into 2 × 2 km squares. Blue stars indicate locations with the highest density of tremor locations for each cluster. Black squares indicate temporary stations, and triangles indicate permanent stations. (a) Density of tremor centroids during the MASE time period. (b) Tremor centroid density during the G-GAP time period. The black contour indicates the 70% tremor activity limit, and the white contour indicates the 50% tremor activity limit.

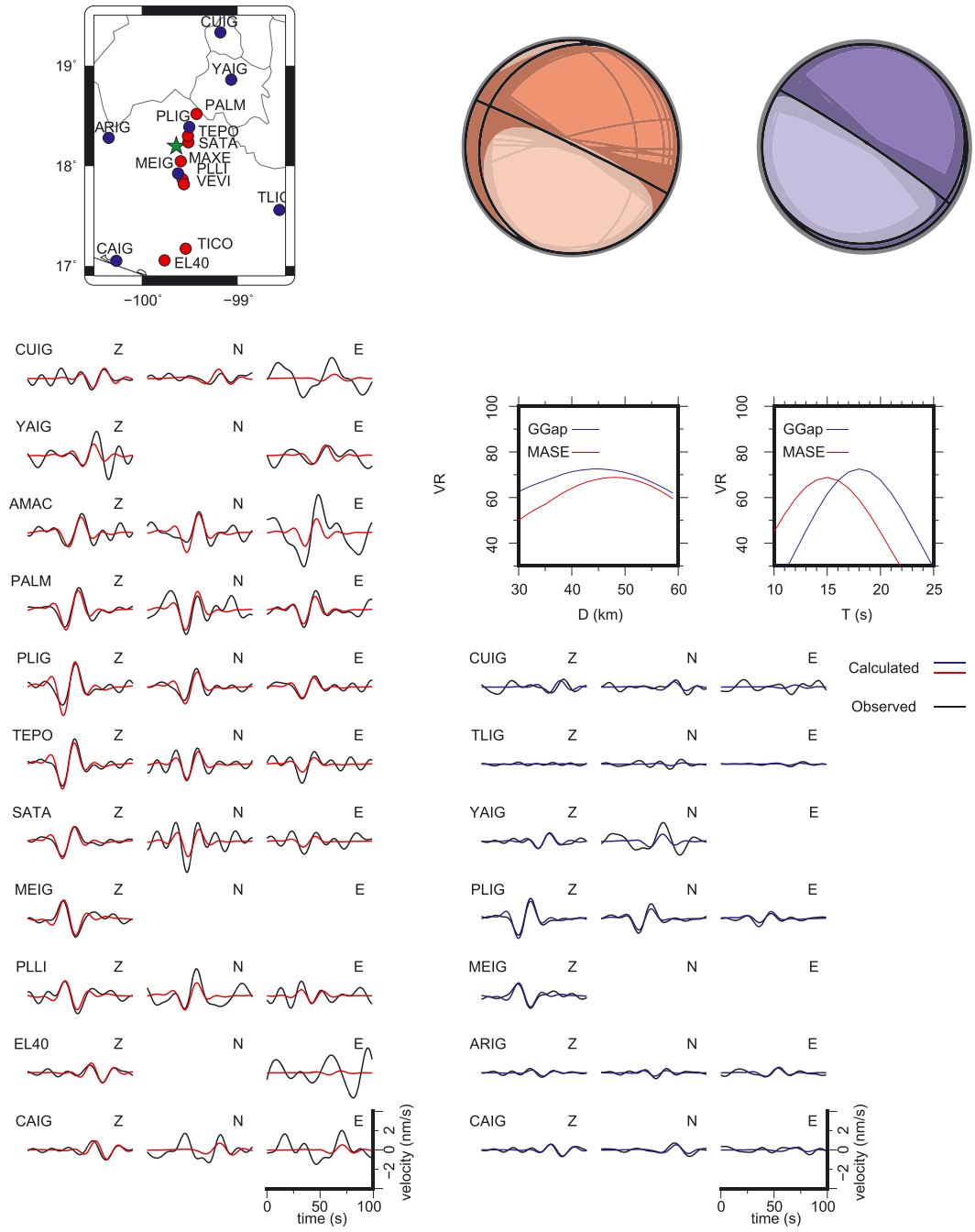

Figure 5. Sample moment tensor inversion for the grid point 18.2°N, −99.6°W for both time periods. (top left) Map view showing the location of the grid point (green star) and stations considered (circles). (Top right) Beach ball representations of the focal mechanism for the MASE time period (red) and G-GAP time period (blue). (middle right) Dependence of variance reduction (VR) on depth and duration. (bottom) Comparison between stacked and calculated (black) waveforms. Waveforms are only shown for components with a nonnull weight.

fact, the longitude of G-GAP tremors is the most well-resolved parameter. As expected, the depth is the least well-resolved parameter. The westernmost and eastern tremor depths are poorly constrained for the MASE time period, which may explain the apparent depth trend in Figure 2c.

To better resolve the spatial variations in the tremor locations, Figure 4 shows the number of tremors within each 2×2 km square of the location region; note that 1σ horizontal location errors are within this range (Figures 3a, 3b, and 3d). The 50% tremor activity contour shows that during the MASE time period the

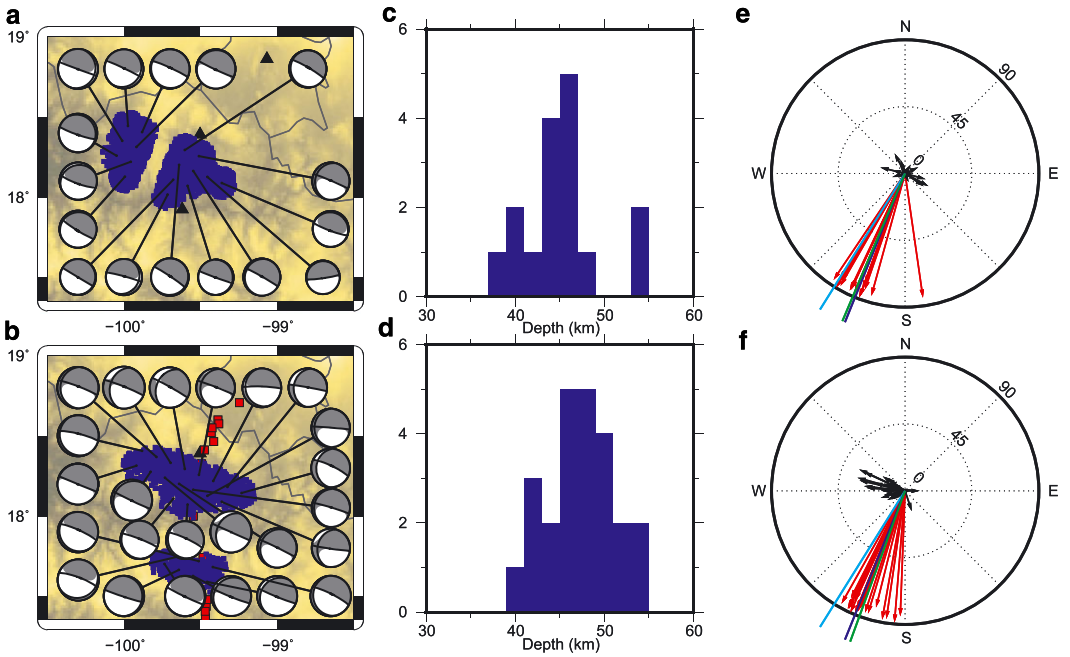

Figure 6. Full results of moment tensor inversions. (top row) G-GAP results and (bottom row) MASE results. (a, b) Beach ball representations of focal mechanisms. (c, d) Histograms of VLF events depths. (e, f) Directions of slip vectors (red) and fault normals (black) are shown as arrows. Green lines show the mean slip direction for each data set, blue lines show plate convergence direction, and cyan lines show dip direction.

sweet spot is composed of two high-density tremor zones in the strike direction, as for the G-GAP time period. The first zone, located next to the MASE stations, is close to the eastern cluster observed during the G-GAP time period and is slightly elongate in the dip direction. The point with the highest number of tremors (in the eastern part of the cluster) is about 13 km west of the point with the highest number of tremors during the G-GAP time period and less than 2 km from the 70% tremor activity contour of Figure 4b. This is relatively close, compared with the 40 km separation of the two G-GAP clusters; consequently, we infer that these two patches are coincident. The second high-density tremor cluster during the MASE time period is elongate in the strike direction and located east of the second G-GAP cluster. This could be related to the previously observed errors in longitude (Figure 3c); it is possible that this cluster is truly located farther west.

As previously shown by *Husker et al*. [2012], the spatiotemporal plot (Figure 2d) indicates that tremors in the transient zone are active mainly during the SSEs, while the sweet spots are persistently active. Even with the G-GAP data set, some activity is seen south of the sweet spots at the time of the SSE (Figure 2d). This activity increases during the second phase of the 2009–2010 SSE, after the Maule earthquake (Figure 2e). Some punctual tremor activity is also seen in the transient zone during the inter-SSE period. This tremor activity is consistent with the LFE activity used to detect short-term slow slip by *Frank et al*. [2015], and the timing of these tremor bursts correspond to the timing of the LFE bursts.

5. Moment Tensor Estimation in the VLF Band

With the MASE data set, 7 focal mechanisms can be estimated in the updip transient zone and 17 in the downdip cluster. Using the G-GAP data, 16 focal mechanisms can be estimated, comprising 9 and 7 solutions for the west and east clusters, respectively (Table S1 in the supporting information). The same numbers of focal mechanisms are estimated in the downdip clusters for the two time periods. Figure 5 shows an example of well-constrained solutions for both data sets. A total of 261 tremors are stacked for MASE solution and 1003 tremors for the G-GAP solution. The stacking results show well-identified signals on the vertical and horizontal channels. The gray curves, indicating solutions obtained from 1000 times bootstrap resampling of the data, suggest that the focal mechanism solutions are reliable. The focal mechanisms for the other points

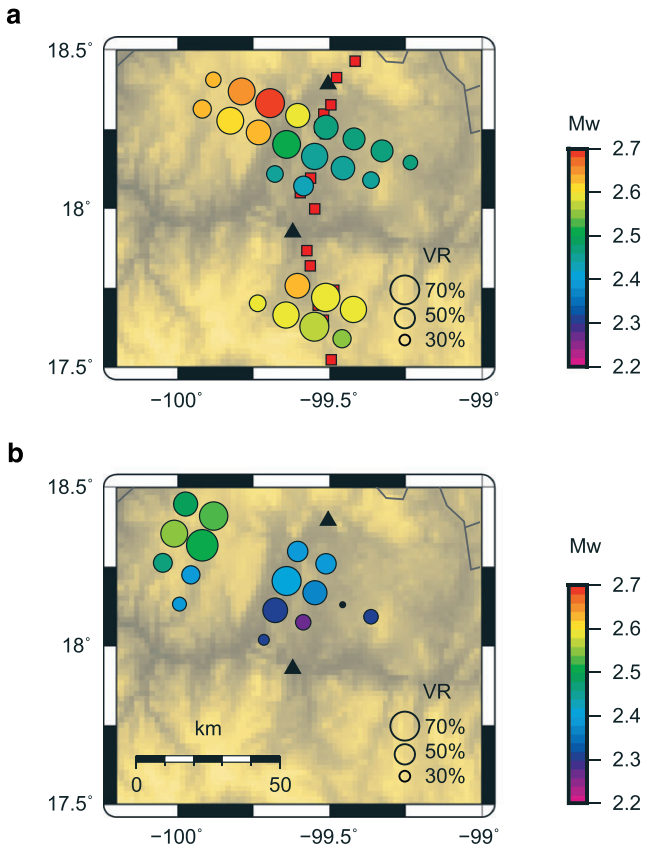

Figure 7. Magnitudes of stacked VLF events, estimated from moment tensor inversion. Size indicates the VR value. (a) Magnitudes of events detected with MASE stations. (b) Magnitudes of events detected with G-GAP stations.

(Figure 6) are also consistent with shear slip on the plate interface. The variance reduction ranges from 20% to 77% for the G-GAP data set and 43% and 73% for MASE data set, comparable to values obtained for VLF signals in Japan [*Ide and Yabe*, 2014]. The low minimum variance reduction for the G-GAP time period is probably due to the low number of available stations, which naturally reduces the signal-to-noise ratio, particularly when few tremors are available. The slip direction is similar between the two time periods, with only a few degrees of difference (N200°E and N204°E, respectively). These values are consistent with the plate convergence direction of N212°E.

No variations in focal mechanism orientations or depths are observed between clusters. On the other hand, some variations in fault plane orientation are observed between the two time periods. While the fault planes for the G-GAP time period are nearly horizontal, and thus consistent with the subduction interface geometry, some inclination is commonly seen in the MASE time period, with a normal oriented N290°E and a dip of 20–35° (Figure 6f). This is similar to the observed trend in depths of tremor hypocenters. As the latter appears to be an artifact of network geometry, this fault plane inclination is probably also an artifact.

The average depth of these VLF events is a little deeper than the plate interface, estimated at about 43 km for this area [*Kim et al.*, 2010]. However, considering depth as a function of variance reduction for a well-determined solution (Figure 5), we see uncertainty in our depth determination.

VLF magnitudes range from 2.2 to 2.6, and estimated durations, *T*, range from 14 to 20 s. These values are comparable with, or slightly smaller than, those estimated for VLF signals in western Japan [*Ide and Yabe*, 2014]. For G-GAP data, the magnitudes in the transient zone are slightly larger than the magnitudes of events in the sweet spots (Figure 7). This relationship is less clear for the MASE results in the sweet spot, but the events closer to the stations all have magnitudes of 2.4, i.e., the same magnitude as the colocated G-GAP events. This magnitude is also lower than 2.6, i.e., the magnitude of events within the transient zone. Events with the larger magnitude located within the sweet spots are farther from the stations; hence, their solutions might be poorly constrained. These variations between clusters suggest that the size of VLF events varies along dip.

6. Matched Filter Detection and Characterization of Additional VLF Signals

Our observations of simultaneous VLF signals and tremors do not necessarily imply that VLF signals are always accompanied by tremors. This is important because we suppose tremors and VLF earthquakes are different expressions of the same phenomena. While statistically this assumption seems justified, it remains to be verified for individual events. To check whether VLF earthquakes can occur alone, we try to detect them independently of tremor bursts using a matched filtering algorithm.

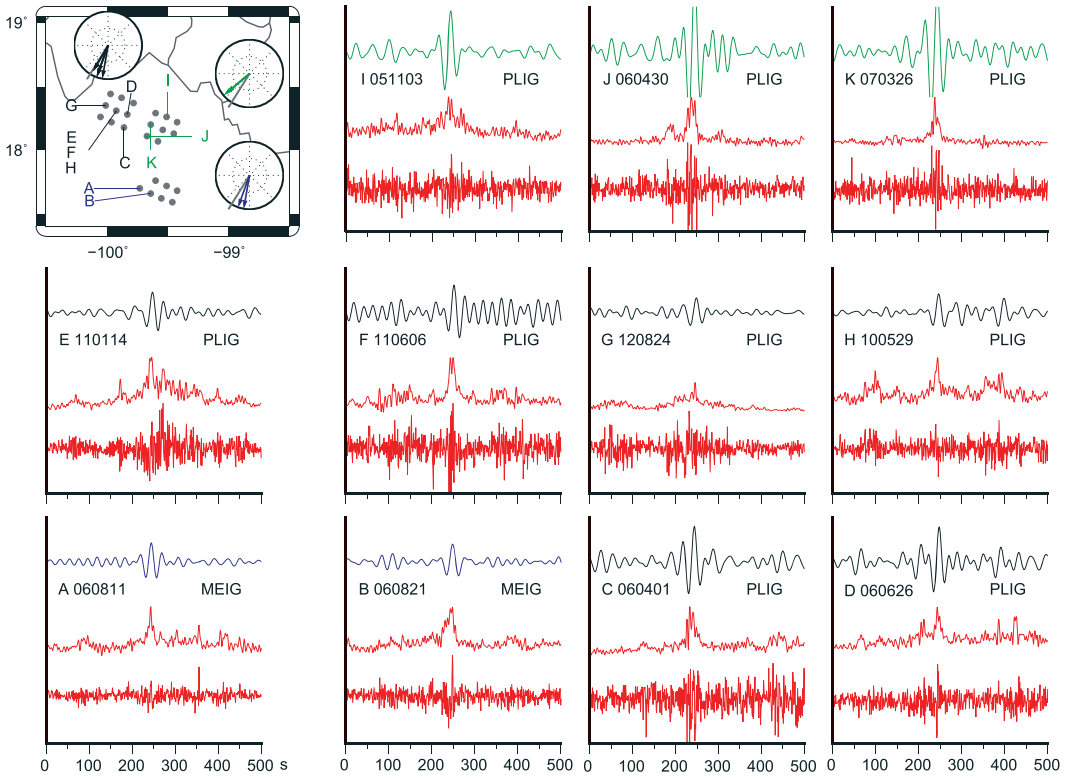

Figure 8. Results of VLF signal detection. (top left) Slip direction for each cluster. The points used in the grid search are shown as grey dots. (middle) Waveform for each event. The red signal is filtered between 2 and 8 Hz, and the corresponding red envelope is shown above it. The blue, black, and green signals show the VLF component. Blue traces correspond to the transient zone cluster, black to the western sweet spot, and green to the eastern sweet spot. Data from station PLIG are shown for the sweet spots, and data from MEIG are shown for the transient cluster.

We use the stacked VLF signal as a template for this procedure. Only vertical records are used, because the S/N ratio in the horizontal components (Figure 5) is not large enough to enable detection. For this approach, we reduce the number of MASE stations used to 10 (Figure 1), because the computations are too time-consuming when using all MASE stations. Thus, during the MASE time period, these stacked template signals are cross-correlated against the seismograms of permanent SSN stations and 10 MASE stations. A network correlation coefficient (NCC) is then defined for location i at time j:

$$\mathrm{NCC} = \sum\nolimits_s \mathrm{CC}_s, \tag{4}$$

where CC_s is the correlation coefficient at station s.

Only one set of templates (i.e., one point) is considered for each of the three clusters (each cluster in the downdip zone + the transient zone), because the network correlation coefficient shows little variation between consecutive points. The points considered are listed in Table S1 in the supporting information. Seismograms are scanned in 100 s time windows with 1 s interval. If the NCC exceeds 8 for the first time period or 3.5 for the second time period, a detection is declared. These thresholds correspond to a mean value above 0.5 for each data set. To avoid false positive detections from teleseismic earthquakes, detections are checked against the ANSS catalogue. This procedure detects 11 additional VLF earthquakes (Figure 8 and Table S2 in the supporting information), with clear Z component signals. These new VLF events are consistent with the hypothesis that each VLF earthquake is accompanied by a tremor burst (Figure 8). We could not find any VLF event in the absence of tremor.

We now determine event focal mechanisms and evaluate locations in more detail. We only use vertical-component data to determine the hypocenters and moment tensors of each event, which means that the problem is underdetermined. In addition, during the MASE time period we can see that the fault plane is not well resolved (Figure 6f), presumably due to the network configuration. Consequently, for the isolated

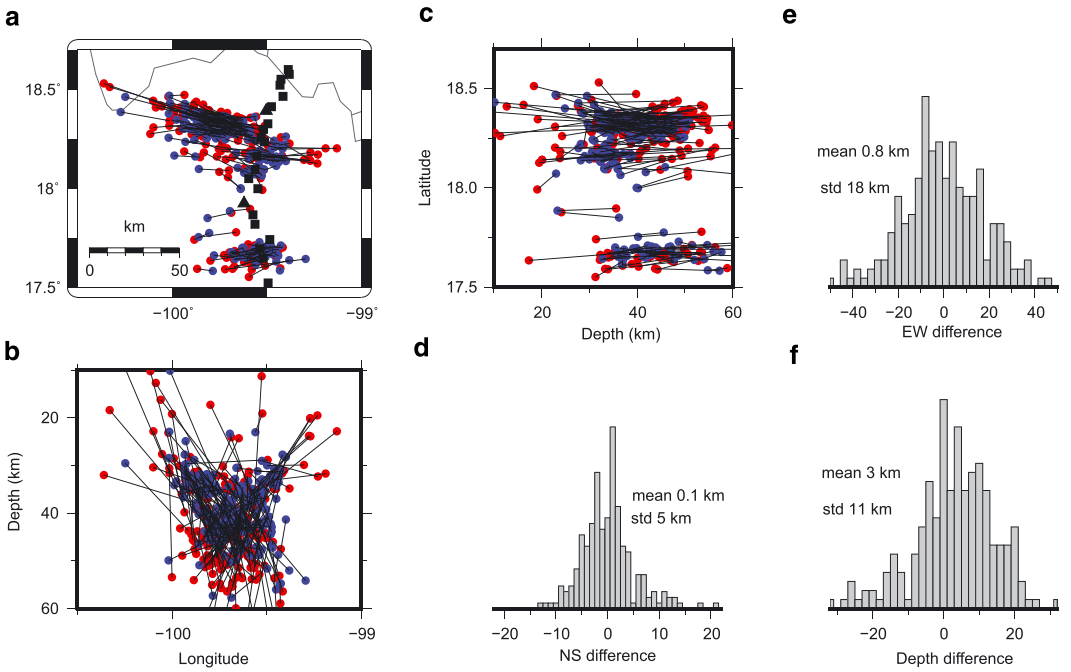

Figure 9. Comparison between tremor hypocenters detected using both horizontal-component data (blue circles) and vertical-component data (red circles). (a) Map view of tremor locations. Locations of each event using horizontal and vertical-component data are connected by black lines. (b) E-W cross section. (c) N-S cross section. (d–f) Histograms of location latitude, longitude, and depth.

VLF events we only attempt to determine a slip direction and magnitude. We impose a dip of 0° or 10° (low-angle fault), a strike of −68°, and a slip direction between −130° and −180° (the main range of values obtained from VLF stacking). To determine the best location and focal mechanism, a grid search is performed to maximize the variance reduction. Every MASE station used in the stacking process is used for the moment tensor determination.

All focal mechanism solutions are low-angle thrusts, as expected from the constraints imposed. The mechanisms themselves are similar, but their slip directions vary a little between clusters, with a mean value of N195° E for the transient zone, N203°E for the western sweet spot, and N230°E for the eastern sweet spot. Event depths vary from 30 km to 54 km, suggesting that this parameter is poorly constrained, even if the variance reduction is relatively high. Their magnitudes are between 3.0 and 3.4, which are similar to observations of VLF signals in Japan [*Ito et al*., 2007] but nearly one unit of magnitude larger than the typical size of VLF events estimated from waveform stacking (mean M_w of 3.2, compared with 2.4). Moreover, the magnitudes of the events located in the transient zone are lower than those of the events within the sweet spot, which is the opposite of the relationship suggested by the stacked waveforms.

7. Discussion

Comparing the MASE and G-GAP data sets allows us to obtain a better picture of how tremor locations in Guerrero relate to tectonics and the source process. The results obtained from the MASE data set, while consistent with previous studies that used the same data [*Payero et al*., 2008; *Husker et al*., 2012; *Frank et al*., 2014; *Cruz-Atienza et al*., 2015], only provide greater resolution along dip. The most recent G-GAP data set reveals that the tremor activity in Guerrero is patchier than previously thought. Careful analysis of the MASE data set seems to confirm this patchy tremor location. Although we have already proposed that different network geometries are probably responsible for the different tremor distributions, there are also differences in the seismic phase types used for each network. We have assumed that tremor is composed mostly of *S* waves, but tremor during the G-GAP time period is detected using principally vertical components of seismograms, which includes a significant contribution of *P* waves.

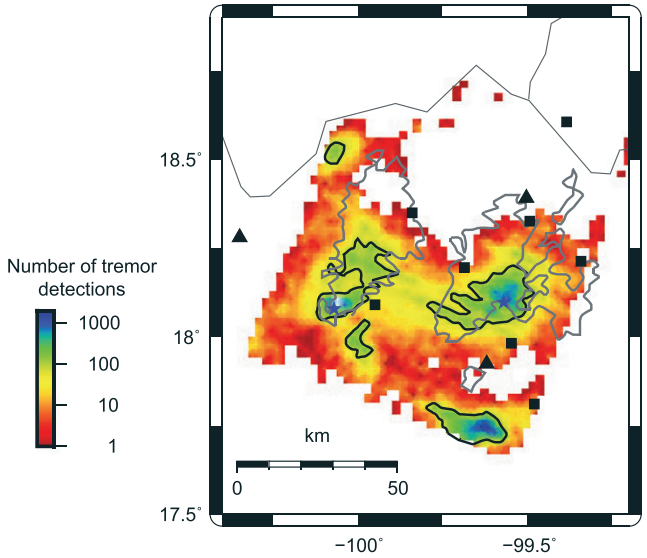

Figure 10. Locations of tremors obtained with the TREP method. Colors represent the number of tremors within 2 × 2 km bins. Black contours indicate the 70% tremor activity limit. The blue stars indicate the locations with the highest density of tremors for each cluster. Grey contours indicate the corresponding activity limits estimated using the envelope correlation method.

To evaluate the impact of restricting locations to vertical-component data, tremor locations are also computed during the MASE time period using the permanent SSN network with vertical-component data from the temporary network. Five times less tremors are detected in the absence of horizontal component data. Tremor locations are also slightly different (Figure 9). While the differences in latitude are small (0.1 ± 5.0 km), the differences in longitude and depth are as large as 0.8 ± 18.0 km and 3 ± 11 km, respectively. These larger errors in longitude are probably due to the linear configuration of the network, since the latitude is well determined; we anticipate that poorly resolved longitudes should not be a problem for the G-GAP time period. Despite the reduced detectability and poorly constrained depths, analysis with only vertical sensors produces similar results.

To confirm the patchy tremor distribution, we compare our results with the tremor locations obtained with the TREP method [*Cruz-Atienza et al.*, 2015]. Since TREP explains the energy spatial distribution and the particle motion polarization azimuth of tremor signals, locations with this method are independent of those yielded by our envelope correlation technique. Because we are interested in the horizontal segmentation of tremors, we constrained the TREP search range to between 40 and 50 km depth. More than 78,000 locations with resolution lengths smaller than 10 km are determined and display three main source clusters (Figure 10), with the southernmost one lying in the transient zone. Locations in the sweet spot are also segmented into two clusters along the trench-parallel direction, with some activity between them (1 order of magnitude lower). Although the maxima of the clusters found with TREP are shifted 10 km SE and 34 km SSW of the corresponding values for envelope correlation, the overall comparison is consistent (i.e., contours of 70% tremor activity significantly overlap in both cases; see gray contours in Figure 10). We therefore conclude that tremor activity during the G-GAP period was segmented in at least two clusters separated by ~40 km from each other in the trench-parallel direction.

While the width of the tremor zone is considerably larger in Guerrero, the patchy distribution of tremors is similar to tremor distribution in Jalisco, in the northern part of the Mexican subduction zone [*Ide*, 2012]. In the southern part of the subduction zone, tremors have been detected in Oaxaca [*Brudzinski et al.*, 2010]. They are also located around 40 km downdip of the SSEs but with a less patchy distribution than in Jalisco. SSEs in Mexico nucleate either in Guerrero or Oaxaca, but they have been observed bridging the gap between the two areas [*Graham et al.*, 2015]. This means that slow deformation is occurring between the two tremor regions and that tremors could also be observed between these areas. It may only be due to the lack of seismic stations that we have not yet found tremor patches in other parts of the Mexican subduction zone (Figure 1). More investigation is needed along the 40 km isodepth contour to confirm this hypothesis.

The along-strike segmentation of tremor activity may reveal small-scale variations in the geometry of the plate interface (i.e., subducted irregularities) and/or in the mechanical properties of the fault zone close to the interface (e.g., gradients in permeability and thus in pore pressure). Temporal changes of the permeability have been proposed to reconcile observations that suggest both transient and heterogeneous fluid content along the Barbados margin decollement [*Saffer and Tobin*, 2011]. There is also geological evidence [*Fagereng*, 2011; *Collettini et al.*, 2011] suggesting that subducted heterogeneities are linked to the slow slip phenomena.

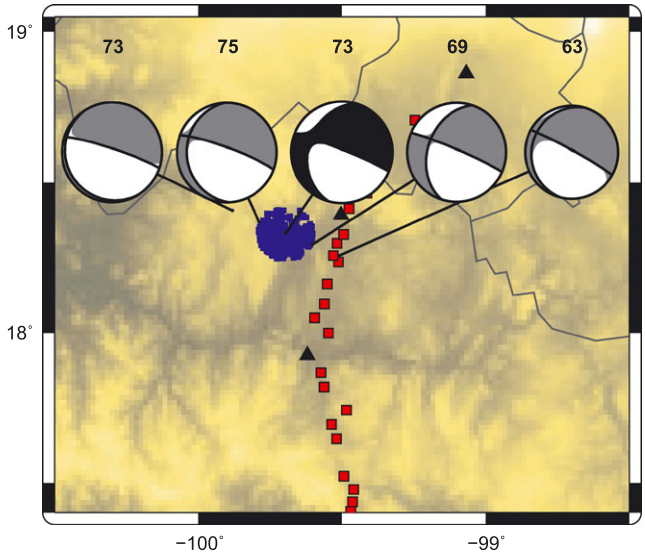

Figure 11. Moment tensor inversions for the stacked tremors located at grid point 18.3°N, −99.7°W, as a function of longitude. The black focal mechanism indicates the result for the grid point where the tremors were located. Each focal mechanism is labeled with its variance reduction.

Numerical modeling studies [*Ando et al.*, 2010; *Skarbek et al.*, 2012] show that heterogeneities in the frictional properties of the plate interface lead to tremor-like behaviors of the dislocation process. The distribution of the heterogeneities would then control the tremor distribution. The diversity of tremor distributions along the Mexican subduction zone from very patchy to nearly continuous would be due to variations in density of the heterogeneities.

A clear increase in tremor detections is seen during the 2006 SSE (Figure 2d), not only in the transient zone but also in the sweet spots as was also seen with LFE activity [*Frank et al.*, 2015]. This is less clear for the 2009–2010 SSE. Some tremor activity is observed south of the sweet spots during this SSE, which is probably related to the tremor in the transient zone. This activity is limited to the 2009–2010 SSE time period, confirming the transient nature of tremor in the updip patch. However, no clear increase in tremor detection is observed in the sweet spots, as for the 2006 SSE. This result may be due to the stations being not yet fully in service during the SSE, but it may also indicate that the sweet spots were not fully activated by the time of this SSE. This could be because the stress perturbation following the Maule earthquake that triggered tremors in the sweet spot [*Zigone et al.*, 2012] activated a short-term slow slip [*Frank et al.*, 2015] and already discharged the sweet spot. An analysis of the time evolution of tremor detections with GPS displacements is needed to confirm this observation.

Some of the focal mechanisms of the VLF events obtained during the MASE time period suggest a variation in the slope of the subduction zone interface, dipping to the west; however, this is not confirmed by the G-GAP results. Considering the uncertainty on the EW location of tremors from the MASE data set, we suspect that this western dip angle is an artifact. In fact, when we move the source location to the east, the dip angle increases to the west (Figure 11), although the variance reductions of the solutions are similar. In conclusion, the fault planes obtained with MASE data are not well constrained, even if the observations are well explained (variance reduction of 73%); only the slip direction seems to be robust. The mechanisms with variations in their fault plane directions coincide with the deeper located tremors and with the area where the second concentration of tremors occurs. This suggests that these events are in fact located farther westward, which coincides with the western cluster of the G-GAP time period.

Analysis of VLF earthquakes in other regions [*Ito et al.*, 2007] indicates that these earthquakes occur as shear slip on the subduction interface. Our results seem coherent with this interpretation, but the depth of the VLF events in this study is slightly greater than the subduction interface and greater than the depths of the LFEs [*Frank et al.*, 2014]. Several structural studies have been undertaken of the Mexican subduction interface [*Pardo and Suarez*, 1995; *Pérez-Campos et al.*, 2008; *Kim et al.*, 2010], and they are generally in agreement with the flat and almost horizontal segment of the interface in Guerrero. However, the depth of this flat segment varies by a few kilometers depending on the model, and our depth estimation has significant uncertainty. Therefore, we cannot definitively conclude whether VLF events occur on the interface or deeper.

VLF magnitudes obtained from waveform stacking vary along the plate interface, with a higher magnitude updip. This is not confirmed by the magnitudes of the independent VLF earthquakes estimates. Since the depths of these events are also highly variable, and there is a trade-off between depth and magnitude, this implies that the magnitude is also poorly constrained. Moreover, the moment tensor estimates obtained from the stacked waveform data give a mean estimate, and some occasional events can be of lower

magnitude. The differences in magnitudes between the moment tensors of stacked and isolated events (mean M_w of about 2.4, compared with 3.2) probably reflect the isolated VLF events being the largest events, although we cannot exclude the possibility that stacked events are affected by waveform misalignment. In addition, the sample of individual events is very small (only two events in the transient zone) so more observations are needed to conclude one way or another on this variation of magnitude.

From analysis of LFEs, mainly before the 2006 SSE, *Frank et al*. [2013] identified a low-angle thrust fault consistent with our observations. They found a slip direction rotated slightly clockwise from the convergence direction; in contrast, our results are rotated anticlockwise by 8–12°. *Cruz-Atienza et al*. [2015] suggested a slip direction subparallel to the convergence direction. Both results are generally consistent with ours. However, we find a slip direction closer to the dip direction than to the convergence direction (Figure 6), even if there is only 10° difference between the two directions. *Radiguet et al*. [2012] found that a slip direction subparallel to the dip direction was more appropriate for the 2006 SSE, in agreement with our results, whereas a slip direction subparallel to the convergence direction better explained the 2009–2010 SSE. Further investigation is needed to corroborate the slip directions of the SSEs; if such a difference is verified, then a component of left-lateral strike-slip movement would be needed to accommodate the stress field.

The data of the two time periods have been fully scanned, but we only find VLF signals during tremors bursts. This suggests that VLF earthquakes do not occur in the absence of tremors. The same suggestion has been made for Japan [*Ito et al*., 2007; *Takeo et al*., 2010]. Due to the high levels of noise in the VLF band, however, our VLF catalog is not complete for this region. Thus, it is still possible that undetected, isolated VLF earthquakes occurred.

8. Conclusions

The envelope correlation method was used to study nonvolcanic tremors recorded by two different experiments in Guerrero, Mexico. Results show significant variability in tremor locations, depending on the data set. This underlines the importance of adequate network configuration for location techniques. Locations of the more recent G-GAP data set, which had better spatial coverage, reveal that tremor activity in the sweet spot is segmented into two clusters separated by 40 km in the trench-parallel direction. This finding indicates that tremor sources are patchier than previously thought and that other tremor clusters may exist and could be found in Mexico if denser seismic networks were installed. This probably reflects small-scale variations in the interface geometry and/or heterogeneities in fluid content within the fault zone.

Moment tensor solutions obtained from stacked VLF waveforms show focal mechanisms with slip directions close to the plate dip direction. If correct, this means that some left-lateral strike-slip deformation is being accommodated in the continental plate. The best resolved focal mechanisms are consistent with a subhorizontal fault plane with depths close to the depth of the subduction interface. The magnitudes of these events are generally higher in the transient zone than for the sweet spot clusters. This variation is similar to that observed in other subduction zones.

Routine and independent detection of VLF earthquakes only reveals events during tremor activity. This suggests that VLF events only occur during tremor bursts, similar to the LFEs or tremors that are concomitant with SSE [*Frank et al*., 2014; *Zigone et al*., 2012]. This may, however, be due to catalogue incompleteness.

Acknowledgments

We thank all the volunteers who made the operation of the MASE and G-GAP arrays possible and for the data used in this study (http://www.gps.caltech.edu/~clay/MASEdir/data_avail.html; G-GAP data are available upon request at IsTerre). SSN data were obtained by the Servicio Sismológico Nacional (México), whose staff are acknowledged for station maintenance, data acquisition, and data distribution. The G-GAP experiment was funded by the Agence Nationale de la Recherche (France) under contract RA0000CO69 (ANR G-GAP). GMT software [*Wessel and Smith*, 1991] was used to generate the figures. We thank the Associate Editor and an anonymous reviewer for their helpful comments.

References

Ando, R., R. Nakata, and T. Hori (2010), A slip pulse model with fault heterogeneity for low-frequency earthquakes and tremor along plate interfaces, *Geophys. Res. Lett.*, *37*, L10310, doi:10.1029/2010GL043056.

Ando, M., Y. Tu, H. Kumagai, Y. Yamanaka, and C.-H. Lin (2012), Very low frequency earthquakes along the Ryukyu subduction zone, *Geophys. Res. Lett.*, *39*, L04303, doi:10.1029/2011GL050559.

Beroza, G., and S. Ide (2011), Slow earthquakes and nonvolcanic tremor, *Annu. Rev. Earth Planet. Sci.*, *39*, 271–296, doi:10.1146/annurev-earth-040809-152531.

Brown, J. R., G. C. Beroza, and D. R. Shelly (2008), An autocorrelation method to detect low frequency earthquakes within tremor, *Geophys. Res. Lett.*, *35*, L16305, doi:10.1029/2008GL034560.

Brown, J. R., G. C. Beroza, S. Ide, K. Ohta, D. R. Shelly, S. Y. Schwartz, W. Rabbel, M. Thorwart, and H. Kao (2009), Deep low-frequency earthquakes in tremor localize to the plate interface in multiple subduction zones, *Geophys. Res. Lett.*, *36*, L19306, doi:10.1029/2009GL040027.

Brudzinski, M. R., and R. M. Allen (2007), Segmentation in episodic tremor and slip along Cascadia, *Geology*, *35*(10), 907–910, doi:10.1130/G23740A.1.

Brudzinski, M. R., H. R. Hinojosa-Prieto, K. M. Schlanser, E. Cabral-Cano, A. Arciniega-Ceballos, O. Diaz-Molina, and C. Demets (2010), Nonvolcanic tremor along the Oaxaca segment of the Middle America subduction zone, *J. Geophys. Res.*, *115*, B00A23, doi:10.1029/2008JB006061.

Collettini, C., A. Niemeijer, C. Viti, S. A. F. Smith, and C. Marone (2011), Fault structure, frictional properties and mixed-mode fault slip behavior, *Earth Planet. Sci. Lett.*, *311*, 316–327, doi:10.1016/j.epsl.2011.09.020.

Cruz-Atienza, V. M., A. Husker, D. Legrand, E. Caballero, and V. Kostoglodov (2015), Nonvolcanic tremor locations and mechanisms in Guerrero, Mexico, from energy-based and particle motion polarization analysis, *J. Geophys. Res. Solid Earth*, *120*, 275–289, doi:10.1002/2014JB011389.

Fagereng, A. (2011), Frequency-size distribution of competent lenses in a block-in-matrix mélange: Imposed length scales of brittle deformation?, *J. Geophys. Res.*, *116*, B05302, doi:10.1029/2010JB007775.

Frank, W. B., N. M. Shapiro, V. Kostoglodov, A. L. Husker, M. Campillo, J. S. Payero, and G. A. Prieto (2013), Low-frequency earthquakes in the Mexican sweet spot, *Geophys. Res. Lett.*, *40*, 2661–2666, doi:10.1002/grl.50561.

Frank, W. B., N. M. Shapiro, A. L. Husker, V. Kostoglodov, A. Romanenko, and M. Campillo (2014), Using systematically characterized low-frequency earthquakes as a fault probe in Guerrero, Mexico, *J. Geophys. Res. Solid Earth*, *119*, 7686–7700, doi:10.1002/2014JB011457.

Frank, W. B., M. Radiguet, B. Rousset, N. M. Shapiro, A. L. Husker, V. Kostoglodov, N. Cotte, and M. Campillo (2015), Uncovering the geodetic signature of silent slip through repeating earthquakes, *Geophys. Res. Lett.*, *42*, 2774–2779, doi:10.1002/2015GL063685.

Ghosh, A., J. E. Vidale, J. R. Sweet, K. C. Kreager, and A. G. Wech (2009), Tremor patches in Cascadia revealed by seismic array analysis, *Geophys. Res. Lett.*, *36*, L17316, doi:10.1029/2009GL039080.

Graham, S., C. DeMets, E. Cabral-Cano, V. Kostoglodov, B. Rousset, A. Walpersdorf, N. Cotte, C. Lasserre, R. McCaffrey, and L. Salazar-Tlaczani (2015), Slow slip history for the Mexico subduction zone: 2005 through 2011, *Pure Appl. Geophys.*, doi:10.1007/s00024-015-1211-x.

Husker, A., S. Peyrat, N. Shapiro, and V. Kostoglodov (2010), Automatic non-volcanic tremor detection in the Mexican subduction zone, *Geofis. Int.*, *49*(1), 17–25.

Husker, A. L., V. Kostoglodov, V. M. Cruz-Atienza, and D. Legrand (2012), Temporal variations of non-volcanic tremor (NVT) locations in the Mexican subduction zone: Finding the NVT sweet spot, *Geochem. Geophys. Geosyst.*, *13*, Q03011, doi:10.1029/2011GC003916.

Ide, S. (2010), Striations, duration, migration and tidal response in deep tremor, *Nature*, *466*, 356–359, doi:10.1038/nature09251.

Ide, S. (2012), Variety and spatial heterogeneity of tectonic tremor worldwide, *J. Geophys. Res.*, *117*, B03302, doi:10.1029/2011JB008840.

Ide, S., and S. Yabe (2014), Universality of slow earthquakes in the very low frequency band, *Geophys. Res. Lett.*, *41*, 2786–2793, doi:10.1002/2014GL059712.

Ide, S., G. C. Beroza, D. R. Shelly, and T. Uchide (2007a), A scaling law for slow earthquakes, *Nature*, *447*, 76–79, doi:10.1038/nature05780.

Ide, S., D. R. Shelly, and G. C. Beroza (2007b), Mechanism of deep low frequency earthquakes: Further evidence that deep non-volcanic tremor is generated by shear slip on the plate interface, *Geophys. Res. Lett.*, *34*, L03308, doi:10.1029/2006GL028890.

Ide, S., S. Yabe, H.-J. Tai, and K. H. Chen (2015), Thrust-type focal mechanisms of tectonic tremors in Taiwan: Evidence of subduction, *Geophys. Res. Lett.*, *42*, 3248–3256, doi:10.1002/2015GL063794.

Iglesias, A., S. K. Singh, A. R. Lowry, M. Santoyo, V. Kostoglodov, K. M. Larson, and I. Franco-Sánchez (2004), The silent earthquake of 2002 in the Guerrero seismic gap, Mexico ($M_w = 7.6$): Inversion of slip on the plate interface and some implications, *Geofis. Int.*, *43*(3), 309–317.

Iglesias, A., R. W. Clayton, X. Pérez-Campos, S. K. Singh, J. F. Pacheco, D. García, and C. Valdés-González (2010), *S* wave velocity structure below central Mexico using high-resolution surface wave tomography, *J. Geophys. Res.*, *115*, B06307, doi:10.1029/2009JB006332.

Imanishi, K., T. Uchide, and N. Takeda (2016), Determination of focal mechanisms of nonvolcanic tremor using *S* wave polarization data corrected for the effects of anisotropy, *Geophys. Res. Lett.*, *43*, 611–619, doi:10.1002/2015GL067249.

Ito, Y., K. Obara, K. Shiomi, S. Sekine, and H. Hirose (2007), Slow earthquakes coincident with episodic tremors and slow slip events, *Science*, *315*, 503–506, doi:10.1126/science.1134454.

Ito, Y., K. Obara, T. Matsuzawa, and T. Maeda (2009), Very low frequency earthquakes related to small asperities on the plate boundary interface at the locked to aseismic transition, *J. Geophys. Res.*, *114*, B00A13, doi:10.1029/2008JB006036.

Kao, H., S.-J. Shan, H. Dragert, G. Rogers, J. F. Cassidy, and K. Ramachandran (2005), A wide depth distribution of seismic tremors along the northern Cascadia margin, *Nature*, *436*, 841–844, doi:10.1038/nature03903.

Kennett, B. L. N., E. R. Engdahl, and R. Buland (1995), Constraints on seismic velocities in the Earth from travel times, *Geophys. J. Int.*, *122*, 108–124.

Kim, Y., R. W. Clayton, and J. M. Jackson (2010), Geometry and seismic properties of the subducting Cocos plate in central Mexico, *J. Geophys. Res.*, *115*, B06310, doi:10.1029/2009JB006942.

Kostoglodov, V., S. K. Singh, J. A. Santiago, S. I. Franco, K. M. Larson, A. R. Lowry, and R. Bilham (2003), A large silent earthquake in the Guerrero seismic gap, Mexico, *Geophys. Res. Lett.*, *30*(15), 1807, doi:10.1029/2003GL017219.

Kostoglodov, V., A. Husker, N. M. Shapiro, J. S. Payero, M. Campillo, N. Cotte, and R. Clayton (2010), The 2006 slow slip event and nonvolcanic tremor in the Mexican subduction zone, *Geophys. Res. Lett.*, *37*, L24301, doi:10.1029/2010GL045424.

La Rocca, M., K. C. Creager, D. Galluzzo, S. Malone, J. E. Vidale, J. R. Sweet, and A. G. Wech (2009), Cascadia tremor located near plate interface constrained by *S* minus *P* wave times, *Science*, *323*, 620–623, doi:10.1126/science.1167112.

Larson, K. M., V. Kostoglodov, S. Miyazaki, and J. A. S. Santiago (2007), The 2006 aseismic slow slip event in Guerrero, Mexico: New results from GPS, *Geophys. Res. Lett.*, *34*, L13309, doi:10.1029/2007GL029912.

Meso-American Subduction Experiment (2007), Meso-America Subduction Experiment (MASE), dataset, doi:10.7909/C3RN35SP.

Nadeau, R. M., and D. Dolenc (2005), Nonvolcanic tremors deep beneath the San Andreas Fault, *Science*, *307*, 389–389, doi:10.1126/science.1107142.

Obara, K. (2002), Nonvolcanic deep tremor associated with subduction in Southwest Japan, *Science*, *296*, 1679–1681, doi:10.1126/science.1070378.

Obara, K., H. Hirose, F. Yamamizu, and K. Kasahara (2004), Episodic slow slip events accompanied by non-volcanic tremors in southwest Japan subduction zone, *Geophys. Res. Lett.*, *31*, doi:10.1029/2004GL020848.

Outerbridge, K. C., T. H. Dixon, S. Y. Schwartz, J. I. Walter, M. Protti, V. Gonzalez, J. Biggs, M. Thorwart, and W. Rabbel (2010), A tremor and slip event on the Cocos-Caribbean subduction zone as measured by a global positioning system (GPS) and seismic network on the Nicoya Peninsula, Costa Rica, *J. Geophys. Res.*, *115*, B10408, doi:10.1029/2009/JB006845.

Pardo, M., and G. Suarez (1995), Shape of the subducted Rivera and Coco plates in southern Mexico: Seismic and tectonic implications, *J. Geophys. Res.*, *100*(B7), 12,357–12,373, doi:10.1007/s004100050129.

Payero, J. S., V. Kostoglodov, N. Shapiro, T. Mikumo, A. Iglesias, X. Pérez-Campos, and R. W. Clayton (2008), Nonvolcanic tremor observed in the Mexican subduction zone, *Geophys. Res. Lett.*, *35*, L07305, doi:10.1029/2007GL032877.

Peng, Z., and K. Chao (2008), Non-volcanic tremor beneath the Central Range in Taiwan triggered by the 2001 M_w 7.8 Kunlun earthquake, *Geophys. J. Int.*, *175*, 825–829, doi:10.1111/j.1365-246X.2008.03886.x.

Peng, Z., and J. Gomberg (2010), An integrated perspective of the continuum between earthquakes and slow-slip phenomena, *Nat. Geosci.*, *37*, 599–607, doi:10.1038/NGEO940.

Pérez-Campos, X., Y. Kim, A. Husker, P. M. Davis, R. W. Clayton, A. Iglesias, J. F. Pacheco, S. K. Singh, V. C. Manea, and M. Gurnis (2008), Horizontal subduction and truncation of the Cocos plate beneath central Mexico, *Geophys. Res. Lett.*, *35*, L18303, doi:10.1029/2008GL0351127.

Radiguet, M., F. Cotton, M. Vergnolle, M. Campillo, B. Valette, V. Kostoglodov, and N. Cotte (2011), Spatial and temporal evolution of a long term slow slip event: The 2006 Guerrero slow slip event, *Geophys. J. Int.*, *184*, 816–828, doi:10.1111/j.1365-246X.2010.04866.x.

Radiguet, M., F. Cotton, M. Vergnolle, M. Campillo, A. Walpersdorf, N. Cotte, and V. Kostoglodov (2012), Slow slip events and strain accumulation in the Guerrero gap, Mexico, *J. Geophys. Res.*, *117*, B04305, doi:10.1029/2011JB008801.

Rogers, G., and H. Dragert (2003), Episodic tremor and slip on the Cascadia subduction zone: The chatter of silent slip, *Science*, *300*, 1942–1943, doi:10.1126/science.1084783.

Royer, A. A., and M. G. Bostock (2014), A comparative study of low frequency earthquake templates in northern Cascadia, *Earth Planet. Sci. Lett.*, *402*, 247–256.

Saffer, D. M., and H. J. Tobin (2011), Hydrogeology and mechanics of subduction zone forearcs: Fluid flow and pore pressure, *Annu. Rev. Earth Planet. Sc.*, *39*, 157–186, doi:10.1146/annurev-earth-040610-133408.

Schwartz, S. Y., and J. M. Rokosky (2007), Slow slip events and seismic tremor at circum-Pacific subduction zones, *Rev. Geophys.*, *45*, RG3004, doi:10.1029/2006RG000208.

Shelly, D. R., G. C. Beroza, S. Ide, and S. Nakamura (2006), Low-frequency earthquakes in Shikoku, Japan, and their relationship to episodic tremor and slip, *Nature*, *442*, 188–191, doi:10.1038/nature04931.

Shelly, D. R., G. C. Beroza, and S. Ide (2007), Non-volcanic tremor and low-frequency earthquake swarms, *Nature*, *446*, 305–307, doi:10.1038/nature05666.

Skarbek, R. M., A. W. Rempel, and D. A. Schmidt (2012), Geologic heterogeneity can produce aseismic slip transients, *Geophys. Res. Lett.*, *39*, L21306, doi:10.1029/2012GL053762.

Takeo, A., et al. (2010), Very broadband analysis of a swarm of very low frequency earthquakes and tremors beneath Kii Peninsula, SW Japan, *Geophys. Res. Lett.*, *37*, L06311, doi:10.1029/2010GL042586.

Wech, A. G., and K. C. Creager (2007), Cascadia tremor polarization evidence for plate interface slip, *Geophys. Res. Lett.*, *34*, L22306, doi:10.1029/2007GL031167.

Wessel, P., and W. H. Smith (1991), Free software helps map and display data, *Eos Trans. AGU*, *72*(41), 441–446, doi:10.1029/90EO00319.

Zigone, D., et al. (2012), Triggering of tremors and slow slip events in Guerrero, Mexico, by the 2010 M_w8.8 Maule, Chile, earthquake, *J. Geophys. Res.*, *117*, B09304, doi:10.1029/2012JB009160.